Daylight operation of a sodium laser guide star for wave front sensing

Stuart Jefferies
Department of Physics and Astronomy, Georgia State University, Atlanta, GA 30303
and Institute for Astronomy, University of Hawaii, 34 Ohia Ku Street, Pukalani, HI 96768
Michael Hart
College of Optical Sciences, University of Arizona, 1630 E. University Blvd., Tucson, AZ 85721
and Institute for Astronomy, University of Hawaii, 34 Ohia Ku Street, Pukalani, HI 96768
Douglas Hope
US Air Force Academy, Dept. of Physics, 2354 Fairchild Dr., Colorado Springs, CO 80840
Neil Murphy
Jet Propulsion Laboratory, California Institute of Technology, Pasadena, CA 91109

ABSTRACT

Current high-resolution ground-based optical observations of resident space objects are largely limited to night-time because of the difficulty of seeing objects against the daylight sky. Atmospheric aberration correction becomes very challenging because photon noise from Rayleigh-scattered sunlight obscures the signal from all but the largest and brightest targets. However, the problem can be alleviated, to a large extent, by using a laser guide star (LGS) that is located above the dominant layers of atmospheric turbulence and that can be detected with a good signal-to-noise ratio against a bright sky. In this paper we show that a sodium-LGS viewed through a magneto-optical filter fulfills these requirements. We also provide a formalism that allows tomographic wave-front estimation from a single beacon, and provides a way to mitigate the focus anisoplanatism inherent in the LGS signal due to its finite height in the atmosphere.

1 MOTIVATION

A LGS is an effective means to extend the sky coverage and scientific value of AO systems operating at astronomical telescopes. Indeed, most large observatories around the world now employ beacons generated by resonant backscatter of laser light at the D_2 line of 589.16 nm from atomic sodium in the mesosphere. In 2001, Beckers and Cacciani suggested that the value of extremely large telescopes (ELTs) in the 25 m class and larger could be extended by using them to make high-resolution observations in thermal infrared wavelengths during the day [1] since the limitation imposed by the bright sky background in these bands is no worse than at night. While there are of course serious practical challenges to operating a large telescope when the Sun is above the horizon, there is also a significant advantage. The scientific return on the substantial investment in ELTs, which is now being made, could be roughly doubled by operating them essentially around the clock. The same method can add value to SSA telescopes of a more conventional size operating in the EO/IR bands. RSOs normally observable only in terminator mode may be imaged during the day, enormously relieving present constraints on their accessibility from the ground and improving the timeliness of data products. Indeed, there are classes of Sun-synchronous objects that are currently all but unobservable from any given telescope site that will finally be brought within reach.

What is needed is a tool to allow the LGS to be used effectively when seen against the bright sky background at the beacon wavelength. Beckers and Cacciani noted that placing the WFS behind a sodium atomic vapor filter could do this. Such filters are referred to in the literature as Faraday anomalous dispersion optical filters (FADOF) or magneto-optical filters (MOF). Here we adopt the MOF naming convention. The MOF has a number of desirable characteristics including high throughput and wavelength stability, and wide angular acceptance. Most importantly, it offers a bandpass of less than 10 pm, which is sufficiently narrow to block almost all the scattered sunlight but wide enough to admit all the LGS light [2].

2 DAYLIGHT LASER GUIDE STAR EXPERIMENT

The University of Arizona (UA) has a sodium laser on long-term loan from the US Air Force Research Laboratory. The laser generates approximately 6.5 W of narrow-band continuous-wave light in a beam that is circularly polarized to take advantage of optical pumping [3]. It is installed on an optical bench next to the UA's 1.5 m Kuiper

telescope on Mount Bigelow in Arizona. The beam has a Gaussian profile and is launched through a 10 cm aperture that is separated from the Kuiper telescope's optical axis by approximately 5 m. For the experiment described in this paper, the laser launch projector was pointed at zenith, and the Kuiper telescope pointed slightly off zenith to place the sodium resonance beacon at about 90 km range within its field of view. A simple instrument bolted to the Cassegrain focus of the Kuiper telescope included an imaging camera behind a sodium MOF from the Eddy Company (Apple Valley, California). We used this arrangement to evaluate the potential for using a sodium LGS for daytime wave front sensing.

The basic MOF consists of a cell that contains an atomic vapor placed between crossed linear polarizers in a kilogauss-level magnetic field. The magnetic field results in both Zeeman splitting of the atomic resonance lines in the vapor and a variation of the polarization-dependent absorption coefficient and refractive index (anomalous dispersion) with wavelength across the vapor absorption lines. A suitable choice of vapor temperature and magnetic field strength results in the absorption and birefringence profiles producing wavelength-dependent transmission in the vicinity of the resonance lines through rotation of the polarization [4]. At the wavelength of peak transmission, a linearly polarized beam with axis aligned to the first polarizer will be rotated in the vapor cell to align precisely with the axis of the second polarizer. Under these conditions, the theoretical transmission maximum for the MOF configuration used in the work reported here (longitudinal magnetic field strength 3.7 kG, temperature 167°C) is close to 100% (Fig. 1) without accounting for transmission losses in the optics. To maximize the LGS signal at our detector we placed a high-transmission (T=0.995) zero-order quarter-wave plate (QWP) in front of the MOF to convert the circularly polarized return laser light into linearly polarized light with the axis aligned to the first polarizer of the MOF.

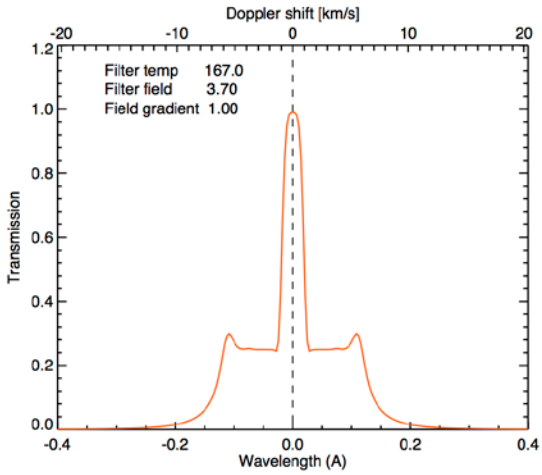

Fig. 1. Theoretical transmission curve for linearly polarized light at the entrance window of a MOF with a longitudinal magnetic field strength of 3.7 kG, operating at a temperature of 167°C.

Practically, a narrow-band interference filter is required in front of the MOF to suppress off-band leakage through the polarizers. The measured transmission curve of the optics of our MOF with the vapor cell cold and polarizers uncrossed has a width of 2.8 nm, determined by the interference filter, and a peak of 0.5. This is commensurate with the manufacturers' transmission values for the components: 0.82 for the polarizers, 0.75 for the narrow-band interference filter, and 0.995 for each of the windows of the sodium vapor cell. For detection we use a Point Grey Flea3 camera in 12-bit mode. To allow us to compute absolute photometry of the LGS, we determined the mean gain of the camera by measuring a photon transfer curve [5]. The result of 2.96 e-/ADU is in good agreement with the manufacturer's specification of 3.0 e-/ADU.

After acquiring the LGS on the imaging camera, we focused the 1.5 m telescope at the height of the mesospheric sodium layer. Continuous sequences of 200–500 images were recorded at 4 frames per second with individual exposure times of 0.25 s. Fig. 2 shows the LGS seen through the MOF in an integration of 8 s, the sum of 32 exposures, recorded during daylight, approximately 42 minutes after sunrise. The LGS has a full width at half maximum (FWHM) of 3.1 arcsec, which is the result of a combination of seeing and diffraction of the Gaussian beam profile at the launch aperture. The image scale on our camera was 0.156 arcsec/pixel, which for analysis was binned by 16× to 2.5 arcsec/pixel.

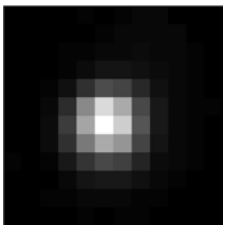

Fig. 2. The LGS seen against the daytime sky at 07:04 local time. The exposure time is 8 s and the pixel scale is 2.5 arcsec.

We observed the characteristics of the LGS from 00:00 local time (07:00 UTC) to 07:04 local time (14:04 UTC) on March 24, 2016. As local sunrise was at 06:22 (13:22 UTC) this provided observations during both nighttime and daytime conditions. The change in contrast between the laser light and the background sky is nicely illustrated in the photographs in Fig. 3.

Fig. 3. (Left) The laser beam propagating to zenith through the slit of the Kuiper telescope dome is easily seen at night. (Right) Approximately the same view in daylight when the beam is very hard to see.

2.1 Daylight LGS Results

Figure 4 shows the LGS and sky brightness as seen through the MOF as the sun rose. The LGS brightness was found to remain approximately constant over the time frame of these observations at a mean value of 1.20×10^6 photon/m/s. This is consistent with previous measurements [6] given our output power at the time of approximately 6.5 W, the low Na column density of 2.5×10^9 cm^{-2} expected in early spring, about half the annual mean [7], and the overall transmission of the system which we estimate to be 0.19. The telescope itself, with two bare aluminum-coated mirrors, has a throughput of ~0.8; the relay optics, comprising two protected silver fold mirrors, an AR-coated collimating lens and the QWP, contribute a factor of 0.95, the measured transmission of the MOF is 0.44, and the Flea3 quantum efficiency at 589 nm is quoted by the manufacturer to be 0.56. This would imply a flux at the telescope aperture of 1.0×10^6 photon/m/s/W, although we note that the uncertainty in this estimate is not quantified. We note that polarizers with higher transmission are available. In addition, use of 1 nm wide 99% transmission prefilter would increase the transmission of the MOF optics to 0.8.

With the MOF in place, the sky background remains very low throughout the period of the observations at about 1000-1100 photon/m^2/s/arcsec^2 with a slight rise toward the end of the sequence, about 45 minutes after sunrise. Unfortunately, observations had to cease at that time to avoid subjecting the telescope head ring to direct sunlight.

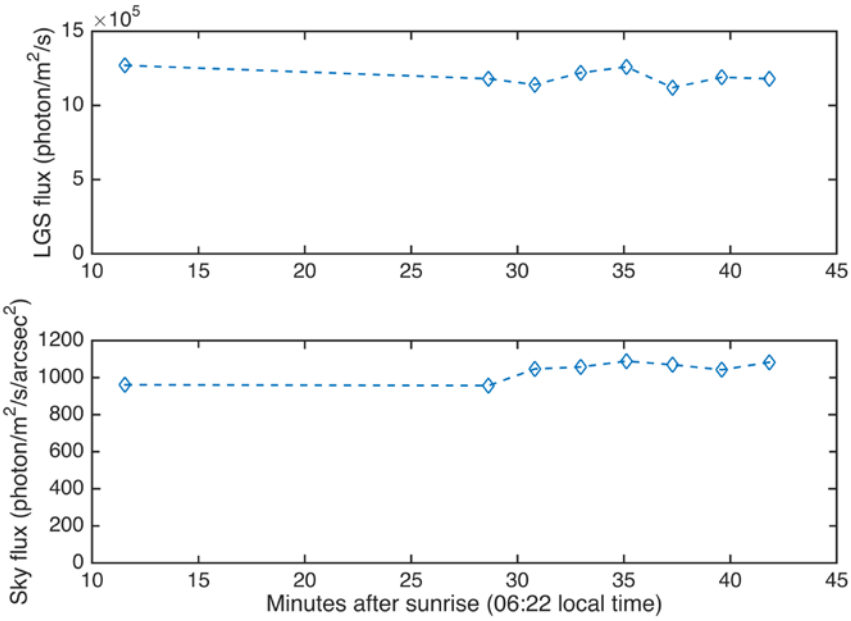

Fig. 4. (Top) Flux from the LGS in the period after sunrise. (Bottom) Simultaneous measurements of the background flux from the sky.

3 ATMOSPHERIC TOMOGRAPHY WITH A SINGLE LGS

WFS systems that rely on a LGS are subject to focal anisoplanatism arising because the volume of air sampled by the beacon at finite range differs from that encountered by a more distant object. At an observing wavelength λ the error is quantified, in physical length units, by $\lambda/2\pi(D/d_0)^{5/6}$ where D is the telescope diameter and d_0 defines the strength of focus anisoplanatism [8]. Particularly for imaging at visible wavelengths focus anisoplanatism is typically the dominant error term. For example, at the AEOS telescope with d_0=2 m at 500 nm wavelength, the error is about half a wave.

To overcome focus anisoplanatism and achieve blur-free imagery, the wave front must first be characterized over the volume of atmosphere between the scene and the telescope. Present techniques to do so rely on multiple beacons, either natural stars or laser guide stars, to probe the atmospheric aberration along different lines of sight, followed by tomographic projection of the measurements. Here we show that a three-dimensional estimate of the wave-front aberration can be recovered from measurements by a single guide star provided that the telescope tracks across the sky with non-uniform angular velocity. This is generally the case for observations of artificial earth-orbiting satellites.

Instead of relying on multiple sight lines through the turbulent atmosphere, we exploit the fact that the aberration is strongly correlated on short time scales. We use the frozen flow model (FFM), which treats the evolution of the aberration as a series of independent static layers, each moving across the telescope aperture with the prevailing wind at the altitude of the layer. Because of its simplicity, the FFM is frequently used as the basis for numerical studies of telescope imaging performance, particularly in the modeling of AO systems. While the FFM is observed not to hold in the real world over long time scales, a number of studies [9-11] have shown that it is a reasonable approximation for short but still interesting periods. For example, from observations made at the 1.5 m telescope of the Starfire Optical Range, at 0.74 μm wavelength, Schöck & Spillar [11] found that the FFM is a good approximation for a time scale τ_{FFM} of 20 ms or less. The accuracy degraded over time such that after 100 ms only 50% of the temporal evolution of the wave front could be described by the FFM. Nevertheless, the period of validity of the model, τ_{FFM}, is an order of magnitude longer than τ_0, the expectation value of the time required for the phase of a wave front in a circular telescope aperture to change by 1 radian rms [8].

In the very simple and artificial case of aberration characterized by a single frozen but wind-blown layer, it is easy to see that taking WFS data at two different times along the same line of sight can yield tomographic information in the

same way as two simultaneous measurements along different lines of sight. The equivalent angular separation of the sight lines θ_s in the former case is $v_l\, t_{WFS}/h_l$ where the quantities are respectively the wind speed v_l at the layer, the elapsed time t_{WFS} between frames of the WFS, and the range of the layer h_l from the telescope. In standard multi-beacon tomography, θ_s is set by the geometry of the optical system and is known. However, in the single-beacon case, only t_{WFS} is known. To recover the same wave front information one must estimate both v_l and h_l.

We begin with an analysis of the WFS data to determine the number of layers of significant atmospheric aberration and their apparent velocity through the telescope's light path. The technique, described in detail by Hope et al. [12], relies on the 3D spatio-temporal autocorrelation of the wave front slopes calculated from the signals of a Shack-Hartmann WFS. The signature of a frozen layer is a line of high correlation radiating from the origin. The angles made by the line with respect to the zero spatial-lag axis in the autocorrelation cube are determined by the apparent wind vector of the layer. The coherence time τ_{FFM} for the layer is estimated from the rate of decay of the correlation along the line, and although we do not use this information, the power in the line indicates the strength of the aberration. Fig. 5 shows a number of consecutive time-lag slices from an autocorrelation cube calculated from WFS data recorded at the AEOS 3.6 m telescope. Peaks can be seen that correspond to three distinct layers above the telescope, as well as other peaks which do not lie on lines coming from the origin and reflect random correlations.

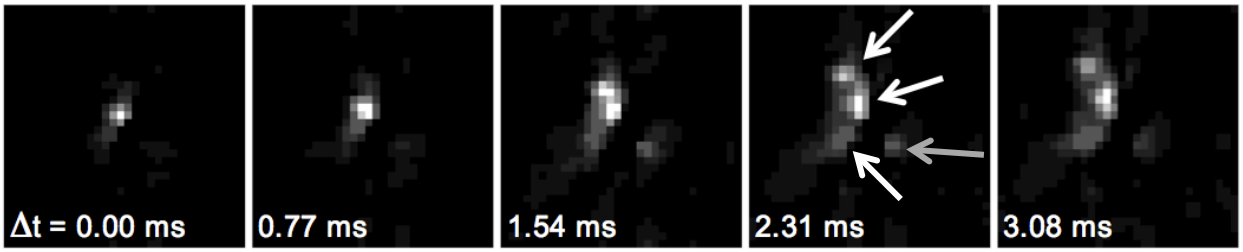

Fig. 5. Consecutive time-lag slices from the 3D autocorrelation of Shack-Hartmann WFS data. The three white arrows indicate correlation peaks corresponding to frozen aberration layers propagating with different velocities. The shaded arrow indicates a random peak not associated with a frozen layer.

In the next step [12], we employ a non-linear least-squares technique in a partial separation of the wave-front gradients on the layers we have identified. The estimates are constrained to match the WFS data in both space and time. Phases at each layer are then calculated from the gradients in the usual way. (Although not germane to tomography, the spatial sub-sampling afforded by the motion of each layer allows us to recover phase estimates on spatial scales shorter than the Nyquist limit imposed by the size of the WFS sub-apertures [13].) We have built a small simulation to show this layer separation. Four atmospheric layers having different strengths, wind vectors, and heights were modeled with frozen Kolmogorov turbulence, as illustrated in Fig. 6. A sequence of 1000 phase screens in the pupil of a telescope of 4 m diameter was made by propagating the layers in time, and light from a beacon through the layers. The beacon was taken to be at 90 km range, the approximate height of a sodium LGS. The WFS was modeled as a Shack-Hartmann with a grid of 32×32 sub-apertures running at 1300 frames per second. The parameters of the model atmosphere are listed in Table 1. The effective value of the Fried coherence length r_0 at 500 nm wavelength was 9.7 cm, and the coherence time τ_0 was 2.0 ms. The mean height of the aberration was 5400 m, giving an isoplanatic angle of 1.1 arcsec.

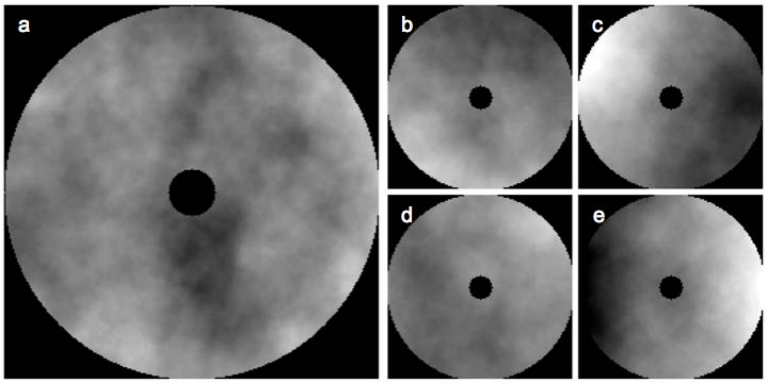

Fig. 6. Single frame from the atmospheric simulation. Combined aberration a is the sum of the four layers b through e.

Table 1. Parameters of the Model Atmosphere

Layer	r_0 (cm)*	Height (m)	Direction	Speed (m/s)
1	17	0	0°	2
2	20	500	0°	10
3	30	5000	-10°	25
4	30	15000	40°	50

*Value of the Fried parameter at 500 nm wavelength.

At this point, although the short-term frozen flow character of the atmosphere has allowed us to determine the number of significant layers of aberration and to distinguish the detailed moment-by-moment contributions, we have still not established the layer ranges, and so cannot make use of our knowledge to mitigate either angular or focal anisoplanatism. The ranges are not uniquely constrained by the data. We can break the degeneracy however if observations can be made with the telescope tracking at two different angular velocities.

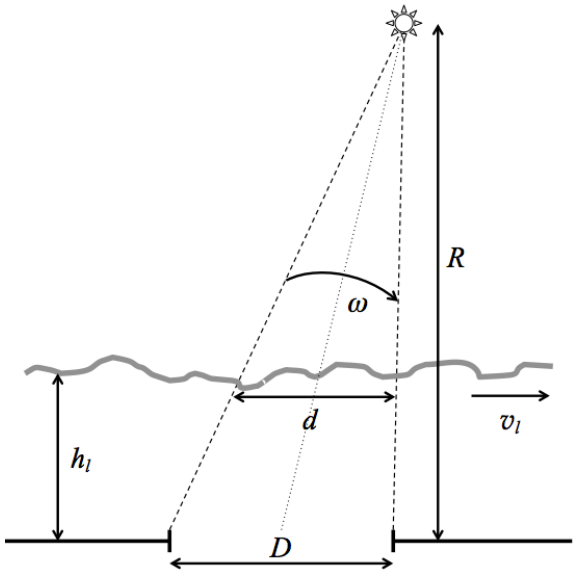

Fig. 7. Wave-front sensing geometry analyzed in this paper. A LGS at range R illuminates a telescope of diameter D. A layer of atmospheric aberration at height h_l propagates with speed v_l. The LGS beam footprint at the layer has diameter d. The telescope tracks with angular speed ω.

Referring to Fig. 7, we start by writing the time t_c for a point on a single layer to cross the telescope beam:

$$t_c = d / \left| \vec{v}_r \right| \tag{1}$$

where superscript arrows represent vector quantities. The beam footprint diameter $d = D(1–h_l/R)$, and the resultant velocity of the beam through the layer is given by

$$\vec{v}_r = \vec{v}_l - \vec{\omega} h_l . \tag{2}$$

Hence,

$$t_c = \frac{D(1 - h_l / R)}{(v_l^2 + \omega^2 h_l^2 - 2 v_l \omega h_l \cos A)^{1/2}} \tag{3}$$

where A is the angle between the wind vector and the direction of motion of the beam induced by the telescope tracking.

The value of t_c for each layer is measured from the autocorrelation of the WFS data. But there are three unknown quantities in Eq. 3: h_l, v_l, and A. To find all of them we make two measurements of t_c with different values of ω, and also observe the change in the angle of each layer's motion through the beam. That is, the tomographic problem can be fully solved if the telescope tracks at a non-constant rate, provided that the layer ranges and velocities do not change significantly during the observations.

The measurement geometry is illustrated in Fig. 8. Solving the triangles in terms of the known and measured quantities is quite straightforward, and leads to a layer height

$$h_l = \left[\frac{\phi}{D} + \frac{1}{R} \right]^{-1} \tag{4}$$

where

$$\phi = t_{c1} t_{c2} \left[\frac{\omega_1^2 + \omega_2^2 - 2\omega_1 \omega_2 \cos B}{t_{c1}^2 + t_{c2}^2 - 2 t_{c1} t_{c2} \cos C} \right]^{1/2} . \tag{5}$$

Finding the actual layer velocities v_l, if needed, is equally straightforward.

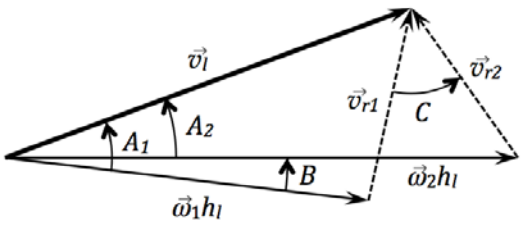

Fig. 8. Vector geometry of the apparent velocities v_1 of the guide star footprint through a layer at height h_l moving with velocity v_l for two telescope track rates ω_1 and ω_2.

We have tested the estimation of layer heights using our four-layer simulation. We assumed telescope tracking rates ω_1 and ω_2 of 0.2°/s and 0.4°/s, typical for low earth orbit satellites, with a 10° difference in direction. The apparent layer velocities and crossing times were determined by the autocorrelation algorithm from our simulated Shack-Hartmann WFS data. The actual and measured values of the crossing times and orientation shift (angle C in Fig. 8) are given in Table 2. The recovered estimates of the layer heights and velocities are shown in Table 3. These are to be compared with the true values in Table 1.

Table 2. Actual (*Measured*) Values of Apparent Layer Wind Vectors in Simulation.

Layer	C (°)	t_{c1} (ms)	t_{c2} (ms)
1	0.0 (*0.1*)	2000 (*1620*)	2000 (*1818*)
2	-5.3 (*-0.7*)	482 (*470*)	604 (*690*)
3	-102.0 (*-104.2*)	451 (*481*)	265 (*276*)
4	54.2 (*54.3*)	95 (*96*)	50 (*52*)

Table 3. Results of Layer Parameter Estimation

Layer	Height (m)	Direction	Speed (m/s)
1	74	1.2°	2.7
2	750	2.1°	11.0
3	4850	-9.5°	24.0
4	14700	40.4°	49.4

In the case of a satellite tracked with a LGS our goal is to reduce the effects of focal anisoplanatism. This error term comprises three components: aberration at ranges beyond the beacon, unsensed aberration outside the cone defined by beacon light but encountered by light from the more distant object, and radial magnification of the sensed aberration as the beacon cone expands to fill the pupil. Our method does not address the first of these, which in any case is likely to be negligible, but the remaining two may be mitigated by respectively exploiting the FFM and our knowledge of the heights of significant layers.

Several methods have been suggested to take advantage of temporal coherence [14-16], including frozen flow characteristics, for improved wave-front control in AO systems. Here, the FFM allows us essentially to know the atmospheric aberration just outside the beacon light cone even when we cannot directly see it. Of course, we can only estimate aberration actually swept out by the beam footprint; some never will be as illustrated in Fig. 9.

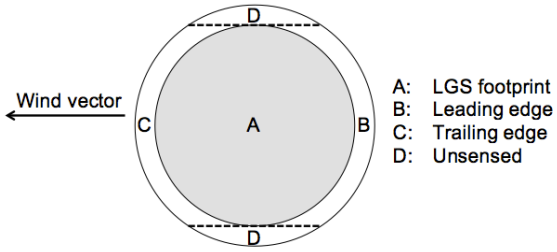

Fig. 9. The beam footprint of the object light (outer circle) on a high-altitude layer is only partially sampled by the LGS (shaded region A) at any given moment. The regions labeled D are never sampled.

Furthermore, in a closed-loop AO system, we can only know past history: the aberration that has already been sampled by the beacon and is now downstream. In that case we may benefit from pointing the laser slightly ahead of the object since in the case of satellites, a significant component of v_r comes from the telescope tracking. In contrast, post-processing applications such as deconvolution from wave-front sensing can take advantage of both future and past history, as we have shown with data taken at the 3.6 m AEOS telescope [12].

By placing the separated layers at their correct ranges, the beam compression ratio h_l/R can be taken into account in deriving the best estimate of the aberration in the object light. The radial magnification arising from the cone effect can be removed. The quantitative reduction in anisoplanatic effects achievable in this way will depend on the prevailing turbulence profile and the extent to which multi-layer frozen-flow behavior can account for the short-term evolution of the wave front. For our model atmosphere in Table 1, the value of the focal anisoplanatism parameter d_0 is 1.9 m [17]. The error itself is 148 nm rms for our 4 m telescope, in satisfactory agreement with the value of

146 nm calculated directly from the 1000 composite phase screens of the simulation. We are able to reduce the error to 54 nm rms by taking advantage of the layer separation and the layer characteristics calculated from tomography in Table 3 to estimate the object phase in regions A, B, and C of Fig. 9. We also explicitly estimate the portions of the object wave front that are not sensed (region D) via a set of 42 disk harmonic modes [18] extending over the full object footprint, but fitted only to the estimated wave front within the LGS footprint.

This result is likely somewhat optimistic since the real atmosphere is not characterized by perfect frozen flow behavior, which we rely on to estimate the phase in regions B and C. For realistic wind speeds and a LGS at 90 km, however, the crossing time for these regions is on the order of milliseconds, an order of magnitude shorter than τ_{FFM}. Focus anisoplanatism typically dominates the wave-front error budget for single-LGS AO systems. We expect that our method will reduce the effect of the error term to the point where that is no longer the case.

4 CONCLUDING REMARKS

We have shown that the scene is set for solving the challenge of wave front sensing during the daytime. Moreover, we have shown that for observations of satellites, tomographic wave front sensing can be achieved with a single LGS. These findings will have a large impact on SSA. While direct sun avoidance will be required, SSA telescopes will be able to collect data continuously during the day, which for LEO objects is now possible only during ~1.5 hour periods near dawn and dusk. This represents a roughly 5× improvement in overall data collection availability for such objects. In addition, SSA observations will be enabled for an important class of sun-synchronous orbits which only appear over a given site during the day and are presently very hard to image at all.

5 ACKNOWLEDGEMENTS

We thank C. Denman and P. Hillman of FASORtronics LLC for their support in operating the laser. We are most grateful to the Mountain Operations team of Steward Observatory for technical assistance with the telescope, and to R. P. Scott for acting as the telescope operator. The United States Air Force Office of Scientific Research under contract FA9550-14-1-0178 and the Air Force Research Laboratory under contract FA9451-12-C-0004 have supported this work. Part of the research and work reported in this paper was carried out at the Jet Propulsion Laboratory, California Institute of Technology, under a contract with the National Aeronautics and Space Administration. The opinions, findings and conclusions expressed in this paper are those of the authors and do not necessarily reflect the views of the United States Air Force.

6 REFERENCES

[1] Beckers, J. M. and Cacciani, A., *Exp. Astr.*, 11, 133, 2001.
[2] Cacciani, A. and Fofi, A. M., *Sol. Phys.*, 59, 179, 1978.
[3] Bienfang, J. C. et al, *Opt. Lett*., 28, 2219, 2003.
[4] Kiefer, W. et al, *Nature Scientific Reports*, 4, 1, 2014.
[5] Janesick, J. R. et al, *Opt. Engr.*, 26, 972, 1987.
[6] Ge, J. et al, *Proc. SPIE*, 3353, 242, 1998.
[7] Papen, G. C. et al, *OSA Technical Digest Series*, **13**, 92, 1996.
[8] Fried, D. L., *J. Opt. Soc. Am. A*, 7, 1224, 1990.
[9] Poyneer, L. A. et al, *J. Opt. Soc. Am. A*, 26, 833, 2009.
[10] Gendron, E. and Léna, P., *Astrophys. Space Sci.*, 239, 22, 1996.
[11] Schöck, E. and Spillar, E. J., *J. Opt. Soc. Am. A*, 17, 1650, 2000.
[12] Hope, D. A. et al., *AMOS Tech.Conf.*, p. E51, 2013.
[13] Jefferies, S. M. and Hart, M., *Opt. Express*, 19, 1975, 2011.
[14] Hinnen, K. et al, *J.Opt.Soc.Am.A*, 24,1714, 2007.
[15] Poyneer, L. and Véran, J.-P., *J. Opt. Soc. Am. A*, 25, 1486, 2008.
[16] Goorskey, D. J. et al, *Opt. Eng.*, 52, 071418, 2013.
[17] Belsher, J. F. and Fried, D. L., *Report TR-576*, The Optical Sciences Company (1984).
[18] Milton, N. M. and Lloyd-Hart, M., *Adaptive Optics: Methods, Analysis and Applications* (OSA Topical Meeting), AWA3, 2005.
[19] Lloyd-Hart, M., *Opt. Lett.*, 27, 1469 (2002).